APPLIED ORGANOMETALLIC CHEMISTRY, VOL. 12, 327–335 (1998)

Nanoporous Aggregates of ZnS Nanocrystallites

S. M. Scholz, R. Vacassy, L. Lemaire, J. Dutta† and H. Hofmann*
Powder Technology Laboratory, Department of Materials Science, Swiss Federal Institute of Technology Lausanne, CH-1015 Lausanne, Switzerland

During the synthesis of ZnS powders by wet chemical precipitation, the formation of nanoporous spheres is observed. The powders have been investigated using thermogravimetric analysis, X-ray diffraction and optical spectroscopies. Nanopore formation can be explained by several stages of growth. The formation of nanoparticles as primary particles is followed by their agglomeration forming secondary particles. These secondary particles are monodispersed spheres with a considerable porosity, because the agglomeration of the nanoparticles is unlikely to be volume-filling. The voids or nanopores formed by this agglomeration process in the secondary particles is estimated to comprise around 35% of the sphere volume. They are mainly filled with water and the residues of the chemical reagents. Water in the pores partially reacts with ZnS and forms hydrated sulphates. The chemical reagents used for the precipitation reactions are also found to be bound to the nanocrystallite's surfaces as ligands in some cases. Depending on the reaction conditions and reagents, the agglomeration of the nanoparticles can also be modified or hindered by the use of complexing agents acting as a sterically stabilizing surface layer on the nanocrystallites. The agglomeration of nanoparticles to larger units being a general phenomenon, this use of complexing agents to control pore formation and agglomerate size should be applicable to other nanocrystalline systems. © **1998 John Wiley & Sons, Ltd.**

Appl. Organometal. Chem. **12**, 327–335 (1998)

Keywords: zinc sulphide; precipitation; nanocrystallites; nanopores; optical transmission spectroscopy; vibrational spectroscopy; Raman spectroscopy; X-ray diffraction; transmission electron microscopy; thermogravimetric analysis

Received 14 November 1997; accepted 5 January 1998

INTRODUCTION

Zinc sulphide, cadmium sulphide and other semiconducting II–VI compounds are applied for a wide variety of technological purposes such as the manufacture of pigments, phospholuminescent screens and optoelectronics. For many of these purposes, particles in the form of powders or colloidal suspensions are used, e.g. to deposit films. The optical and material processing properties are largely dependent on the particle size and form, due to exciton confinement[1] and resonance effects.[2]

Spherical zinc sulphide (ZnS) particles and other related materials such as cadmium sulphide have been synthesized by precipitation from homogeneous solutions. This technique has been studied intensively for ZnS since the mid-1980s.[3] Since then, numerous synthetic methods have been developed, leading to homogeneous size distributions by controlling nucleation or diffusion rates of primary crystallites.[4–7] However, little was known about the internal structure of the spherical particles formed by these reactions except for the size of the primary crystallites and the final particles. Also, most of the surface chemistry of the crystallites remained obscure, though a high content of carbon and oxygen atoms was observed in such particles.[7]

Recently, we have investigated in detail the influence of complexing agents on the particle morphology.[8] It was shown that organic groups may bond to metal atoms on the crystallite surfaces. They are acting as surface ligands and are of the utmost importance for the aggregation behaviour of the primary crystallites. In this work we focus on the porosity created by this aggregation and analyse the organometallic complexes adsorbed on the

* Correspondence to: H. Hofmann, Powder Technology Laboratory, Department of Materials Science, Swiss Federal Institute of Technology Lausanne, CH-1015 Lausanne, Switzerland.
† Current address: Balzers Process Systems, Display Technology Division, P.O. Box 1000, Fl - 9496 Balzers, Liechtenstein.

 CCC 0268–2605/98/050327–09 $17.50

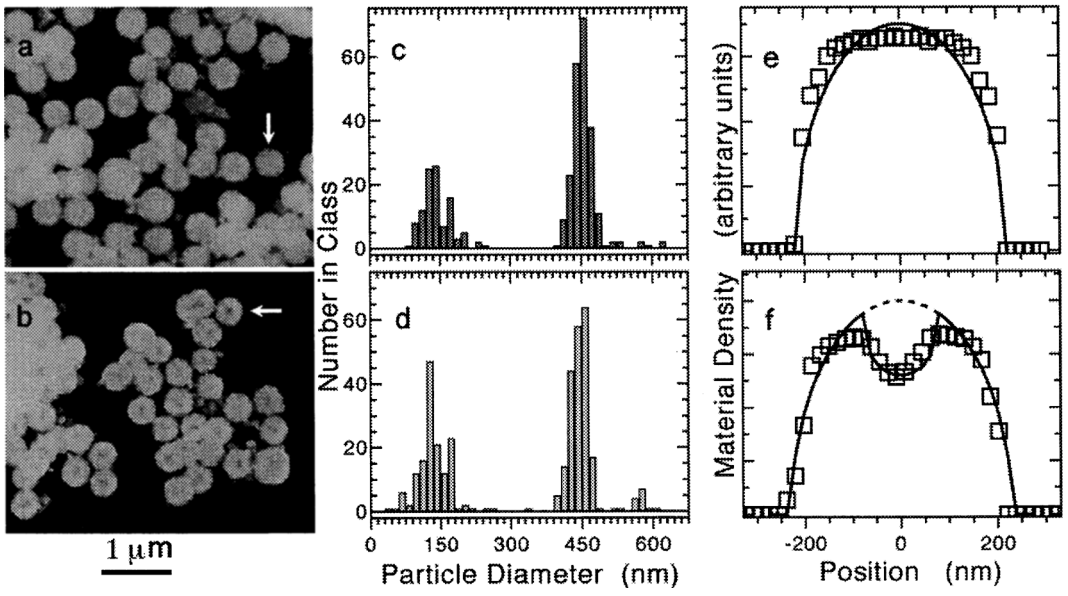

Figure 1 Left: Transmision electron micrographs of ZnS powder as prepared (a) and after annealing at 750 °C in Formier gas (b). Centre: Particle size distribution of as-prepared sample (c) and after annealing to 750 °C (d) as derived from TEM images. Right: Typical brightness profiles of an as-prepared particle (e) and an annealed particle (f). The particles from which the profiles have been taken are marked by the arrows in the micrographs (a,b). The broken and full lines in (e) and (f) represent simulated profiles for solid and hollow spheres, respectively, under the assumption that the brightness is linearly proportional to the mass density.

nanocrystallites and their influence on the particle morphology.

EXPERIMENTAL

ZnS powder was prepared by homogeneous wet chemical precipitation from thioacetamide (TAA) and zinc chloride (ZnCl) in aqueous solution as described in detail elsewhere.[4,5,8] Unless otherwise stated, we refer to the powder produced by this method throughout this paper. Precipitation routes involving other educts and ligands are also described in Ref. 8. All chemicals were of reagent grade and used without further purification. Aqueous solutions were filtered with a 0.2 μm filter before the experiment.

Gas adsorption measurements were performed on Micromeritics Gemini (BET) and ASAP 2010 (BET, BJH) apparatus. Powders were heated in nitrogen (Gemini) or vacuum (ASAP 2010) for some hours before measurements were taken, in order to remove moisture that might clog pores.

Infrared spectroscopy was done on a Nicolet 510 FTIR spectrometer in transmission using KBr pellets. For Raman spectroscopy a DILOR XY800 spectrometer was used with the 514 nm Kr^+ laser line for excitation. Spectra were taken from dry powders.

X-ray diffraction patterns were measured on a Siemens Cristalloflex 801 diffractometer with an angular resolution of 0.05°. Thermogravimetric analysis (TGA) was performed on a Mettler TG50 thermobalance. The heating rate was 5 °C min^{-1} or 10 °C min^{-1}, and the sample was kept in a 20 sccm min^{-1} flow of either N_2 or Formier gas (96% N_2, 4% H_2). The heating compartment was thoroughly rinsed with these gases to reduce oxygen contamination. A commercially available ZnS powder (Sigma) with a milled grain size of several micrometers was used for comparison in some experiments.

Results and discussion

The experimental results obtained from the powders are presented below. First, the experimental methods are discussed which give indications about the particle internal structure. Then the chemical

Table 1 Characteristic sizes for the particles as determined by various experimental techniques[a]

T (°C)	$2r_{TEM}$ (nm)	σ_{TEM} (nm)	$2r_{DLS}$ (nm)	$2r_{XRD}$ (nm)	S_{BET} ($m^2\ g^{-1}$)
As prep.	(i) 457.5 (ii) 142.5	31.3 31.3	450	4.1	4.5
250–350	—	—	—	5.7	50.2
700–800	(i) 449.2 (ii) 132.6	37.1 32.8	—	25	5.2

[a] The particle (agglomerate) diameter $2r_{TEM}$ and polydispersity σ_{TEM} are deduced from TEM images, where two well-separated size modes (i) and (ii) are observed. $2r_{DLS}$ is from dynamic light-scattering measurements. Crystallite diameters $2r_{XRD}$ derived from the XRD peak widths according to Scherrer's equation [1] and specific surface areas S_{BET} are also given.

composition of the non-crystalline material inside the particles is investigated, and a model for the mechanism of nanopore formation is presented.

Particle size determination

Several methods have been utilized to determine particle sizes. Transmission electron micrographs of the powders both before and after thermal treatment to 750°C are shown in Fig. 1(a,b). The particle size distributions derived from these micrographs are reported in Fig. 1(c,d). The size distributions are found to be bimodal in both cases, with the smaller mode representing less than 10% of the total sample volume. The smaller mode may be underestimated from the TEM images, because the particles agglomerated on TEM grids, which may obscure observation of smaller particles more than the larger ones. Nevertheless it is possible to determine mean particle sizes and polydispersities for both modes (see Table 1). The particle size is reduced slightly upon thermal treatment, while the contrast profiles across the spheres suggest a lower-density material enclosed in the larger spheres, i.e. they seem to be hollow shells (Fig. 1f). A hole diameter of 160 nm was estimated from the TEM intensity profiles for a 440 nm sphere. Formation of a hollow centre upon calcination of nanocrystalline ZnS aggregates has already been observed previously.[9]

Dynamic light scattering measurement results also reported in Table I lead to a similar estimation of the particle sizes. Gas adsorption measurements, however, show several interesting features. The BET specific surface area of the as-prepared powder was estimated to be 4.5 $m^2\ g^{-1}$. This value compares well with the specific surface area which one expect on the basis of the particle size distribution in Fig. 1(c). Upon annealing to 200 °C, the specific surface area rises to 12.5 $m^2\ g^{-1}$, and after half an hour at 250 °C in Formier gas the specific surface area rises by one order of magnitude to 50.2 $m^2\ g^{-1}$. BJH analysis indicates that a specific surface area of 47.3 $m^2\ g^{-1}$ arises from the pores, for which an average pore size of 5.3 nm (BET) or 8.5 nm (BJH) is determined. Heat treatment at 750 °C again leads to BET specific surface areas as low as 5 $m^2\ g^{-1}$, which is evidently due to sintering of the grains.

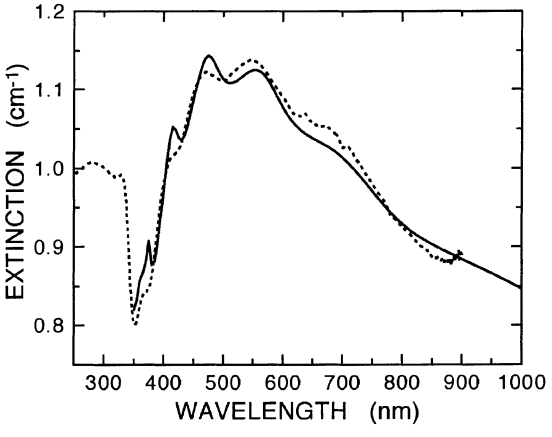

Figure 2 Optical transmission spectrum of colloidal suspension of ZnS spheres in ethanol (broken line) and simulated spectrum from Mie theory under the assumption of porous spherical ZnS particles as scattering objects (full line).

Optical transmission spectroscopy

As the absorption edge of ZnS is at a wavelength of 350 nm, optical transmission spectra of the colloids in the visible and near-infrared range are entirely influenced by elastic scattering effects from the ZnS spheres. Scattering behaviour is mathematically described by Mie theory, leading to complex scattering factors which depend on particle size, refractive indices and the wavelength under con-

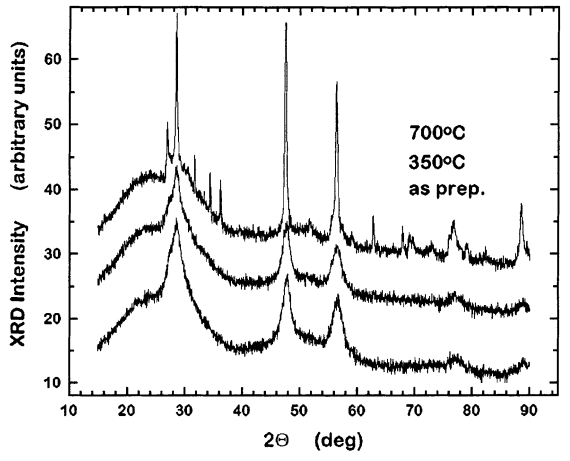

Figure 3 X-ray diffraction curves for ZnS powder as prepared and after annealing at 350 °C and 700 °C in N_2 (from bottom to top). The broad peak between 20° and 30° is due to diffraction from the glass sample holder.

sideration.[10] An example of a typical extinction spectrum is shown in Fig. 2. The extinction curve shows numerous resonance features which can be related to radial and circumference interference modes of the spherical agglomerate. However, a detailed fitting analysis of the spectral lineshape of the extinction spectrum using Mie theory revealed a lower refractive index for the spheres compared with the bulk values as reported in the literature.[2] This can be explained by the existence of porosity in the spheres; according to this analysis, the pores have to be filled with a material of a lower refractive index. For water or materials with a similar refractive index, a 35% volume fraction of filled pores has been found, and the particle size determined from the simulation was $2r_{\mathrm{Mie}} = 476$ nm from the fits. The simulated spectrum is in excellent agreement with the experimental results, as shown in Fig. 2. The particle number density used for this simulation was 1.62×10^8 cm^{-3}.

With a specific weight of 4.0 g cm^{-3} for ZnS and 1.0 g cm^{-3} for water, the 35% volume fraction leads to a weight fraction of about 10% for the nanopore contents. This value would change very slightly, if other materials with a similar specific weight (such as organic components) are assumed to be in the pores. The estimated density of 65 vol% of the spheres agrees fairly well with the value of 57% determined for ZnS particles from Archimedes' method.[9] A detailed description of Mie scattering simulations for ZnS spheres is reported elsewhere.[2]

X-ray diffraction (XRD)

XRD measurements have been used to investigate the crystallization behaviour of the particles (Fig. 3). Spectra were analysed with respect to peak broadening (indicating crystallite sizes) and peak positions (indicating material symmetry).

The XRD spectra from as-prepared particles always show broad peaks at the characteristic positions for ZnS. The FWHM β of the (111) peak for the sphalerite crystal structure was used to estimate the crystallite size of the primary particles. It evolves upon heating from a broad peak with $= 2.2 \pm 0.3°$ for the as-prepared powders to $= 1.6 \pm 0.1°$ after the annealing step to 350 °C. Finally, this peak narrows to $\beta = 0.36 \pm 0.01°$ upon heating the samples to 700 °C. The crystallite sizes $2r_{\mathrm{XRD}}$ corresponding to these broadening values can be roughly estimated using Scherrer's equation

$$2r_{\mathrm{XRD}} = K\lambda/(\beta\cos\Theta) \qquad [1]$$

Here λ is the radiation wavelength of the X-rays and Θ is the diffraction angle. The constant $K = 1$ was used for calculation of the values reported in Table 1. Crystallites are considerably smaller (about half the size) compared with the sizes determined by Han *et al.* for similar powders;[9] this may be due to the fact that samples were kept at elevated temperatures for much longer times in that study. The crystallite size evolution was found to be practically independent of the overall particle (sphere) size. This confirms that the sintering of the particles starts slowly at around 350 °C. It is not surprising that the crystallite sizes which one finally obtains after the process of sintering to 700 °C are independent of any supposed ligands, because these ligands are already evaporated at lower temperatures.

The (111) cubic sphalerite peak at $2\Theta = 28.59 \pm 0.01°$ is in agreement with other reports.[11] An asymmetry, which is visible as a shoulder in the broad peak before calcination, develops into a small peak at $2\Theta = 26.97 \pm 0.01°$. This can be interpreted to arise from material with hexagonal wurtzite symmetry, for which the (100) diffraction peak is expected nearby at $2\Theta = 26.93 \pm 0.01°$.[12] The intensity diffracted into this peak is typically between 5 and 10 times lower than the intensity due to the sphalerite (111) peak position; unfortunately, due to a lack of comparable experimental data, a quantitative estimation of the wurtzite material cannot be done. Some new peaks which appear after the sintering to 700 °C are due to ZnO. Oxygen contamination can be avoided by

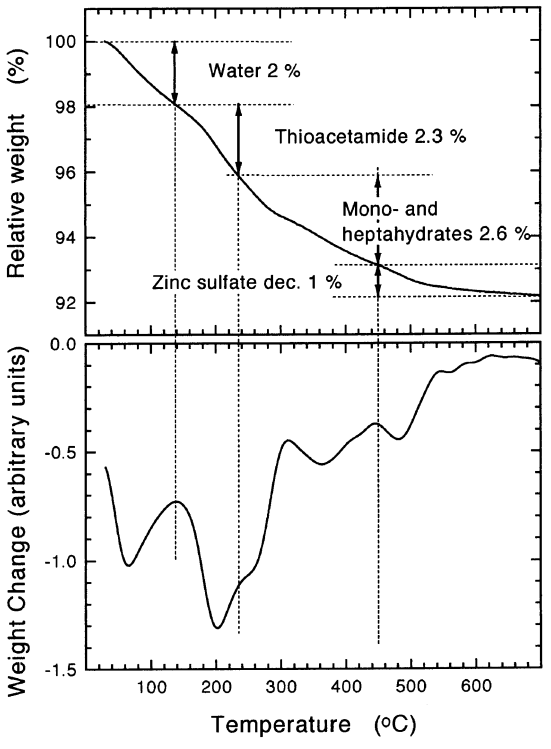

Figure 4 Thermogravimetric analysis curve for ZnS powder precipitated from ZnCl and TAA. Annealing was performed in N_2 at a heating rate of 5 °C min^{-1}. The evolution of sample weight (top) and its derivative (bottom) is shown. Literature values for evaporation and decomposition temperatures of several of the materials involved are assigned to curve peaks.

performing the heating step in a more reducing atmosphere such as N_2/H_2 Formier gas.

Thermogravimetic analysis (TGA)

All ZnS powders lose between 7 and 12% of their weight upon annealing in either N_2 or Formier gases. Depending on the preparation route, the temperatures at which weight losses take place vary. The different desorption or decomposition peaks can be assigned to different species by comparing the temperatures with the characteristic desorption or decomposition temperatures of the materials, which are reported in the literature.[13,14]

For the powder obtained from TAA and $ZnCl_2$ the TGA curves are shown in Fig. 4. The estimated weight fractions of the different identified components are also indicated in the figure. At around 100 °C, water is evaporated. The peak at 210 °C is due to TAA; pure TAA was found to evaporate at 180 °C. In the particles, TAA is assumed to be bonded to nanocrystallite surfaces, which may explain the shift of the desorption peak in Fig. 4. Furthermore, the desorption peak can be shifted due to the small size of the pores, through which the TAA has to make its way to the particle surface. The weight changes between 250 and 450 °C may be mainly due to losses of H_2O from hydrated zinc sulphates, i.e. mono- and hepta-hydrates. Finally, at 500 °C zinc sulphate decomposes. The X-ray results discussed above indicate that during this process some zinc oxide (ZnO) is formed. ZnS and ZnO do not decompose in the temperature range studied here; their melting temperatures are above 1000 °C and 1900 °C, respectively.

Nevertheless, the ZnO fraction can be reduced by using the more reducing Formier gas atmosphere, as was already seen from XRD measurements. Up to temperatures of 500 °C, the weight curves evolve independently of the gas atmosphere. Between 600 and 700 °C, a small peak arises in Formier gas. It may be due to water formation from reduction of ZnO.

A commercial ZnS powder with a grain size of several micrometers which was used for comparison did not show any desorption peak in the whole range; the overall weight change between room temperature and 700 °C was below 0.5%. Once heat-treated up to 700 °C, nanoporous powders also showed negligible hygroscopicity, even after several weeks' storage in ambient conditions. Repetition of the annealing experiment with these powders resulted in relative weight changes of less than 1%, comparable with the pure ZnS reference sample.

The relative amounts of water and other types of contamination vary, depending on the preparation methods. Typically, for each type of contamination (water, TAA, hydrides and sulphates) quantities between 1 and 4 wt% have been found in varying compositions. As mentioned above, the total relative weight loss was always between 7 and 12%. This implies pore volumes between 22 to 35%, respectively, in excellent agreement with the results obtained from Mie scattering analysis.

Vibrational spectroscopy

In order to investigate the chemical characteristics of the material in the pores, the samples were studied by infrared and Raman spectroscopy.

Raman spectra obtained from the dry ZnS powder in air are shown in Fig. 5(a). Experimental

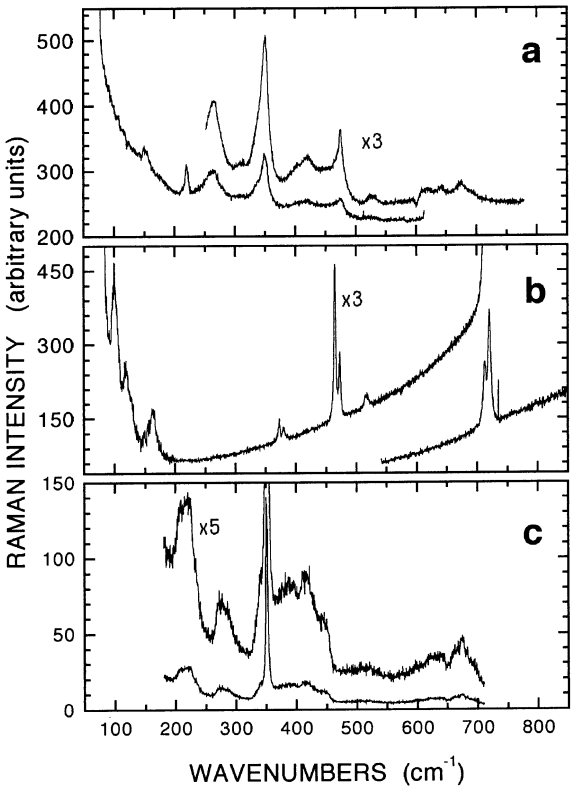

Figure 5 Raman spectra of ZnS spheres precipitated from ZnCl and TAA (a), thioacetamide (b) and a reference sample microcrystalline of ZnS powder (c).

results for peak positions and literature values are compiled in Table 2. The spectra reproduce approximately the peak positions reported in the literature for bulk wurtzite, ZnS.[15,16] Some additional peaks are found which have also been reported by Abdulkhadar and Thomas.[17] In this work, they have been attributed to surface modes of ZnS nanoparticles, which were claimed to have sphalerite structure, and to symmetry-breaking effects; but–with exception of the 475 cm^{-1} peak–these peaks are also emerging in a commercial, micron-sized ZnS powder (Fig. 5c). This indicates that these peaks are not necessarily to be attributed to the nanometric size of the powders as they are also observed for larger grains. For the assignment of the 475 cm^{-1} peak two possibilities can be taken into consideration. On one hand, it is close to the 470 cm^{-1} position where Abdulkhadar and Thomas found a peak for their nanoparticles. On the other hand, a strong peak doublet is observed in thioacetamide at 465 cm^{-1} and 470 cm^{-1} (Fig. 5b), so the observed peak may originate from the TAA bonded inside the particle, probably inside the pores and bonded to the surface of the nanocrystallites. Unfortunately, due to a high photoluminescence background it was not possible to take Raman spectra after heat treatments.

The infrared spectra also indicate the presence of considerable amounts of organic contaminants in the as-prepared samples. Figure 6(B) shows the spectra for powders after heat treatments at different temperatures. The as-prepared powder shows numerous peaks which can be assigned to TAA (Fig. 6A), from their neighbouring spectral positions. The peaks are interpreted by comparison with characteristic group frequencies and the TAA spectrum; peak positions and assignments are compiled in Table 3. Spectra indicate the presence

Table 2 Experimental Raman peak positions for as-prepared ZnS aggregate spheres, comparison and literature values, and their assignment

This work (cm^{-1})	Literature (cm^{-1})	Reference	Assigned to mode
151	150	17	ZnS (nano)
220	216	17	ZnS (nano)
	220	This work	ZnS (micro)
265	273	16	ZnS A_1(TO), E_1(TO)
	274	15	
350	351	16	ZnS A_1(LO), E_1(LO)
	352	15	
420	428	17	ZnS (nano)
	423	This work	ZnS (micro)
475	470	17	ZnS (nano)
	465,470	This work	TAA
525	516	17	ZnS (nano)
674	680	This work	ZnS (micro)

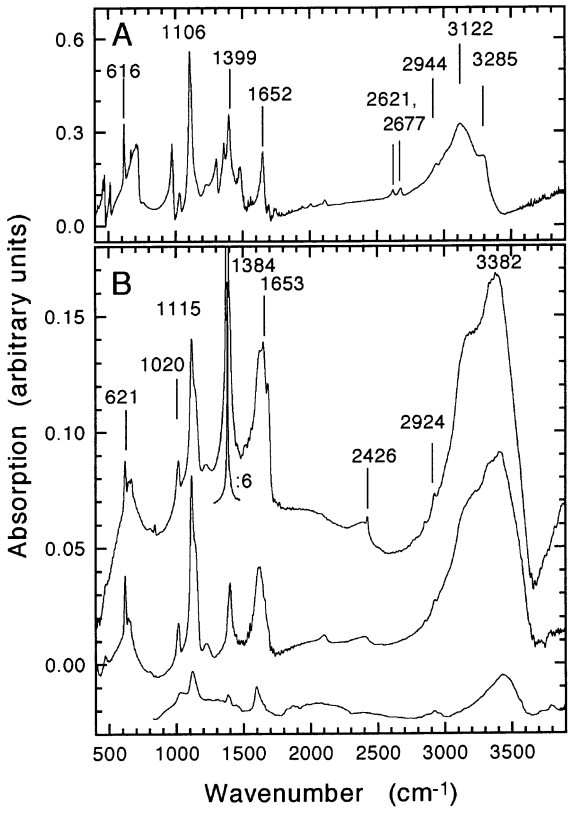

Figure 6 Infrared absorption of thioacetamide (A) and ZnS spheres after different stages of thermal treatment (B). Spectra are shown for as-prepared samples, powder after heating at 200 °C for 30 min in N_2, and after a TGA run to 750 °C in Formier gas (B, from top to bottom). Spectra are normalized for same ZnS content in (B)

of a considerable amount of TAA in the ZnS spheres, with the slight differences from pure TAA in line positions and intensity possibly due to bonding. TAA can exist in two tautomers

$$CH_3–CS–NH_2 \overset{\rightarrow}{\longleftarrow} CH_3–CSH{=}NH$$

with the first one predominant under ambient conditions at room temperature. However, the small peaks found in the 2620–2680 cm^{-1} range in TAA are assigned to an -SH thiol group vibration of the second type; this peak is not found in the ZnS particles, while the N–H-related vibrations persist. It is therefore supposed that in the particles the TAA is not found in its thiol configuration, because it is bonded via the sulphur.

Annealing the powder to 200 °C significantly lowers the dominating -C-CH_3 deformation peak found in the powder at 1384 cm^{-1}. It is not clear why this peak is so intense in the as-prepared powders. To a lower extent, the 1650 cm^{-1} peak, which is partly attributed to water, is also reduced. Surprisingly, the OH-related peak around 3500 cm^{-1} does not diminish visibly though water is assumed to be evaporated in this temperature step.

After heat treatment at 750 °C, absorbance peaks are strongly reduced. Remaining peaks in the 1000^{-1}–1200 cm^{-1} region could arise from sulphate ion resonances. ZnO starts to contribute strong lines to the spectra below 600 cm^{-1} (not shown). The free and bonded -OH groups which are still visible as a peak at wavenumbers up to 3600 cm^{-1} may be re-adsorbed after the heat treatment.

Table 3 Experimental IR absorption peak positions for TAA and the as-prepared ZnS aggregate spheres, with their group mode assignment and desorption temperature range

TAA (cm^{-1})	ZnS as prep. (cm^{-1})	Tentative assignment	Desorption temperature (°C)
616	621	C–S stretching	>200
700	670	C–S stretching or amide band	>200
973, 1027	1020	Organic skeletal vibration, or sulphoxide?	>200
1106	1115	C=S stretching in thioamides, or SO_4^{2-}	>200
1399	1384	C–CH_3 deformation	<200
1652	1653	H_2O or N–H deformation, or C=S stretching in thioesters	~200
—	2426	N–H^+ vibration in $\rangle$C=NH^+	>200
2621, 2677	—	S–H stretching in thiol	>200
2944	2924	C–H stretching	>200
3122	3160	N–H stretching in amide	>200
3285	3382	N–H stretching in =NH or -NH_2	>200
—	3200–3550	O–H stretching	—

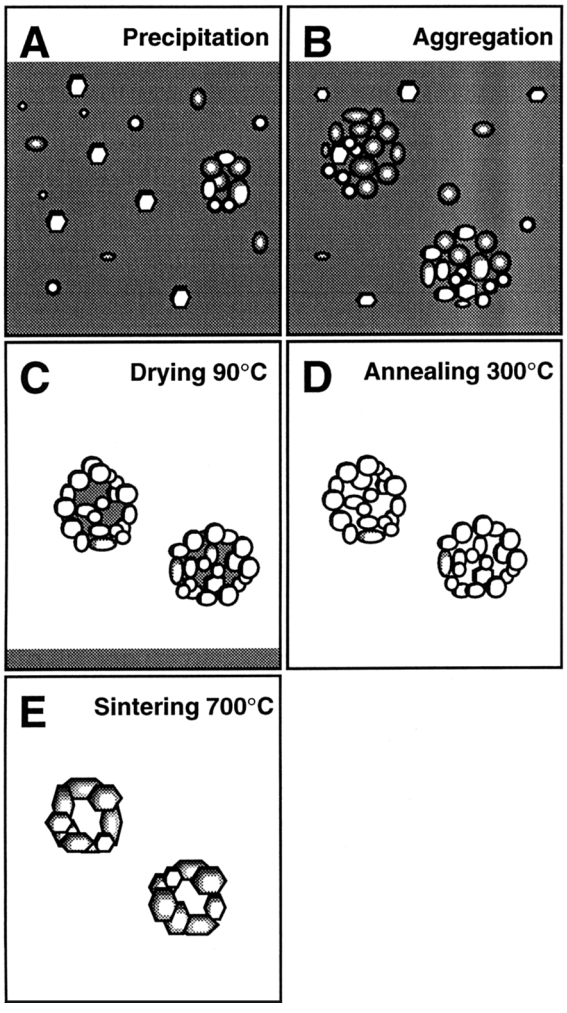

Figure 7 Schematic sketch of the formation of the powder. The nanocrystallites which are precipitating (A) agglomerate to spherical, porous aggregates (B). The aggregate surface is densified upon drying (C). At higher temperatures, trapped materials are evaporated (D). Finally thermal treatment at up to 700 °C leads to sintering and a shell-like structure (E).

Model for nanopore formation

From the observations described above, a complete qualitative model for the description of formation and evolution of the nanoporous structure of the ZnS powders can be formulated. It covers five processing steps which are schematically depicted in Fig. 7.

Precipitation

The first step is the primary nucleation and precipitation of ZnS crystallites in the aqueous solution (Fig. 7A). The crystallite sizes are very small with an upper limit of about 30 nm diameter. That can be justified from the specific surface after annealing. The crystallite size of about 4 nm found by Scherrer's equation is the lower limit, since strain-related broadening in the diffraction spectra cannot be excluded. The crystallite sizes assumed by Celikkaya and Akinc[4] from their calculations are well within these limits. The XRD pattern indicates that the small crystallites are a mixture of hexagonal and cubic phases.

Agglomeration

Once the crystallites are formed, they tend to agglomerate or aggregate in a second step (Fig. 7B), presumably due to van der Waals forces. This is the secondary nucleation leading to the growth of the spheres in the form of a colloidal suspension. Their size distribution stays narrow if post-nucleation can be avoided at this step. This is usually achieved by choosing appropriate (low) primary nucleation rates. The kinetics of this process have been shown to vary significantly, depending strongly on the nature of any chemicals acting as surfactants or ligands.[8] The nanoporosity is created during this step as the aggregating crystallites cannot arrange themselves in a volume-filling way. They agglomerate leaving space between them; as shown by optical Mie scattering analysis, the volume-filling fraction is about 2/3, close to the value for densely packed spheres. This space is filled by other material, i.e. by water (since the reactions are taking place in water) and chemicals, which are also attached to the crystallite surfaces as ligands.

Drying

When these colloidal suspensions are dried (Fig. 7C), moderate temperatures below 100 °C are not sufficient to expel water and other material from the nanopores and from the surfaces where it may be adsorbed. After being dried, the ZnS spheres in fact still contain around 35 vol% of materials other than ZnS hidden in nanopores. By vibrational spectroscopy these materials have been identified as containing ligands stemming from organic precursors. The compressive forces of surface tension may also be responsible for a slight compaction of the spheres' surfaces at this stage, which will have some influence on the sintering behaviour. Water may react with the ZnS nanocrystallite surfaces to form hydrated sulphates.

Evaporation
Heating the powders to temperatures between 200 and 350 °C (Fig. 7D) is finally enough to drive the water out of the nanopores. Ligands are also evaporated at these temperatures, as has been observed by TGA and IR spectroscopy. This step opens the pores of the ZnS aggregates, giving rise to huge changes in specific surface area, by an order of magnitude. At the same time, sintering effects remain negligible, as has been concluded from the XRD measurements.

Sintering
With an annealing step to 700 °C or more, nanocrystallites are sintered (Fig. 7E). The sulphates are decomposed during this heating process. TEM micrographs indicate that the sintered crystallites form a hollow ZnS shell. This is due to a slightly higher density of the sphere surfaces compared with their centers after drying, which was assumed above. TEM micrographs also show that the outer diameter is only very slightly lower than the diameter of the as-prepared powders, while a hole of about one-third of the sphere diameter is found in the center. Some zinc oxide is identified in the powder after this heat treatment from fingerprint XRD peaks. It is not clear if it is a product of the zinc sulphate decomposition, or if it is due to oxygen contamination in the ambient gas during heating.

CONCLUSIONS

This investigation has led to a better understanding of the growth and structure of ZnS spherical particles prepared by precipitation, and the changes which occur due to thermal treatments. Particles have been shown to be nanoporous, with the pores filled with materials trapped during aggregation of the primary nanocrystallites. This material can be evaporated by thermal treatment, thus opening the nanopores. Sintering the spheres at still higher temperatures fused the nanocrystallites to form a hollow spherical ZnS shell. These mechanisms are assumed to be applicable to other materials systems also.

The volume of the nanopores may therefore be taken into consideration for useful applications. For example, the mechanism of incorporation of ligands in the powder can be used to introduce functional groups into the nanopores. Functional groups such as dyes could be attached there during synthesis, to as a sensitizer or emitter for optoelectronics applications. The pore volume can be used for slow drug delivery, because pores retain their contents very effectively. The spheres also allow protected transport of chemicals; for example, hazardous substances or chemicals which would react with their environment if exposed might be enclosed in nanopores. They are then set free by temperature-programmable desorption, e.g. in a hot oil bath.

Acknowledgment Part of this work was supported financially by **Swiss PPM** and **National Fond** programmes.

REFERENCES

1. R. Rosetti, R. Hull, J. M. Gibson and L. E. Brus, *J. Chem. Phys.* **82,** 552 (1985).
2. S. M. Scholz, R. Vacassy, J. Dutta, H. Hofmann and M. Akinc, *J. Appl. Phys.* (1998).
3. D. M. Wilhelmy and E. Matijevic, *Coll. Surf.* **16,** 1 (1985).
4. A. Celikkaya and M. Akinc, *J. Am. Ceram. Soc.* **73**, 2360 (1990).
5. A. Celikkaya and M. Akinc, *J. Am. Ceram. Soc.* **73**, 245 (1990).
6. T. Sugimoto, G. E. Dirige and A. Muramatsu, *J. Coll. Interface Sci.* **180,** 305 (1996).
7. J. D. G. Duran, M. C. Guindo, A. V. Delgado and F. Gonzalez-Caballero, *J. Coll. Interface Sci.* **193,** 223 (1997).
8. R. Vacassy, S. M. Scholz, J. Dutta, C. Plummer and H. Hofmann, *J. Am. Ceram. Soc.* (1998).
9. Y. Han, E. T. Voiles, L. S. Chumbley and M. Akinc, *Proc. Mater. Res. Soc. Symp.* **286,** 99 (1993).
10. H. C. van de Hulst, *Light Scattering by Small Particles*, Dover, New York (1981).
11. H. McMurdie et al., *Powder Diffraction* **1,** 76 (1986).
12. H. Evans and E. McKnight, *Am. Mineral.* **44,** 1210 (1959).
13. S. Budavari (ed.), *The Merck Index*, 11th edn, Merck Rahway, NJ (1989).
14. R. C. Weast (ed.), *CRC Handbook of Chemistry and Physics*, 67th edn, CRC Press, Boca Raton, FL (1987).
15. C. A. Arguello, D. L. Rousseau and S. P. S. Porto, *Phys. Rev.* **181,** 1351 (1969).
16. O. Brafman and S. S. Mitra, *Phys. Rev.* **171,** 931 (1968).
17. M. Abdulkhadar and B. Thomas, *Nanostruct. Mater.* **5**, 289 (1995).

